V-band nanosecond-scale pulse reflectometer diagnostic in the TCV tokamak

P. Molina Cabrera,[1, a)] S. Coda, L. Porte, A. Smolders, and the TCV team[b)]
Ecole Polytechnique Fédérale de Lausanne (EPFL), Swiss Plasma Center(SPC), CH-1015 Lausanne, Switzerland

(Dated: 1 November 2019)

This article describes the realization of a novel approach to short pulse (∼1ns) reflectometry (SPR) recently implemented in the TCV tokamak. Taking advantage of a fast arbitrary waveform generator and vector-network-analyzer extension modules, the design offers flexibility regarding pulse output frequency, duration, and repetition rate. Such flexibility allows the instrument to overcome traditional SPR spatial sampling limitations while reducing hardware complexity. In order to measure the group-delay of ns-scale pulses, both traditional analog and novel digital sampling techniques have been explored. A group-delay range resolution of 17ps (2.6mm) in average over the V-band has been achieved with both timing techniques against a waveguide mirror featuring 10dB power fluctuations. Direct pulse sampling during L-mode plasmas shows that reflected pulse widths increase only by 4% in average. However, pulse width dispersion does occur in L-mode plasmas and leads to an increase in the group-delay uncertainty up to 40ps (6mm). Raw histograms of group-delay data show interesting qualitative changes from L to H-mode. Frequency spectra of group-delay data allow the identification of macroscopic density fluctuations as well as edge quasi-coherent modes during ELM-free H-modes. Lastly, fast changes to the density profile have been measured with microsecond time resolution and sub-cm spatial resolution in both O and X-mode polarizations.

I. INTRODUCTION

In the Tokamak à Configuration Variable (TCV) (a=0.25m, R=0.89m, B_T=1.4T), electron density measurements from the plasma core to the last closed flux surface (LCFS) are routinely available from the Thomson Scattering (TS) diagnostic with a spatial resolution between 6-17mm but only 60Hz temporal sampling. Microwave reflectometry has been identified as a strong candidate for complementary measurements at the edge of confined plasmas given its high spatial (sub cm) and temporal (μs) resolutions. Increasing the temporal resolution of edge density measurements could be decisive in revealing the dynamics of confinement regime transitions and fast pedestal events such as edge-localized modes (ELMs). In microwave reflectometry, the plasma electron density can be inferred from measurements of the round-trip group-delay of EM waves reflected from a plasma cut-off over a number of frequencies. Short pulse reflectometry (SPR) consists of sending broadband microwave pulses (∼1ns) with a defined carrier frequency and measuring their round-trip group-delay using precise chronometers.

SPR is a uniquely attractive approach to reflectometry. Firstly, assuming negligible absorption and weak dispersion, the group-delay of a pulse with a defined carrier frequency can be measured directly. This is in contrast with continuous-wave frequency modulation (CW-FM) techniques where the linearity of frequency sweeps is vital to measure accurate group-delays[1]. Secondly, pulse propagation through the plasma occurs in the ns-scale, at least 2 orders of magnitude under turbulence time scales expected in the sub-μs scale: the plasma can be considered to be truly *frozen* during pulse propagation. Lastly, given the time-domain nature of SPR measurements, spurious reflections in waveguides, vacuum windows, and in-plasma coherent back-scattering can be separated from the plasma cut-off reflection and easily filtered.

SPR does also feature unique technical challenges. SPR prototypes were successfully demonstrated by Shevchenko et al.[2], Heijnen et al.[3], and Tokuzawa et al.[4] in the nineties but none are operational today. SPR was traditionally implemented by combining a discrete number of fixed frequency oscillators, sending sequential ns-scale pulses of increasing frequency, and measuring the round-trip group delays using analog pulse-detection systems. The fixed oscillator frequencies entailed unavoidable frequency gaps of 4-14GHz, which represented an important spatial sampling limitation over CW-FM systems[5]. Every data point in the reconstructed profile required at least one separate oscillator, thus, increasing the number of points in the reconstructed profile meant a linear increase in hardware complexity. Finally, pulses were created by fast semiconductor (PIN) switches which featured insertion losses at the 7dB level and relatively short lifetimes.

The frequency signature of the SPR signal presents unique challenges and opportunities. Pulse envelope dispersion and distortion have been alluded to by many authors[5,6] and studied theoretically[7,8], but, prior to this publication, have not been directly measured. Heijnen[3] (p. 29) showed that, within the WKB approximation, pulses of durations above 0.5ns should not feature pulse dispersion when sampling smooth quadratic density profiles. This result was later confirmed by full-wave 1D simulations in a wider range of profile shapes by Hacquin et al.[7]. Pulse dispersion/distortion has the potential of reducing the accuracy of group-delay measurements, as

[a)] pedro.molina@epfl.ch
[b)] See author list of S. Coda et al 2019 Nucl. Fusion **59** 112023

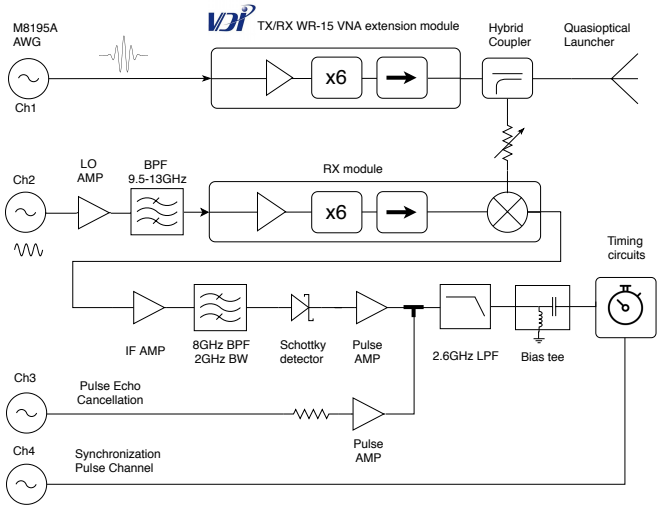

FIG. 1: AWG-driven SPR schematic diagram

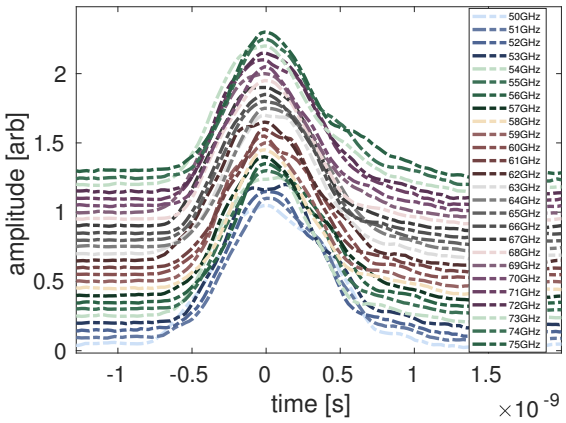

FIG. 2: WR-15 zero-bias Schottky diode data demonstrating that Gaussian pulses of 650-750ns FWHM may be created by an AWG driving x6 VDI varactor multipliers.

further addressed in section IV A. However, if the pulse output width can be varied and the reflected pulse width measured, pulse dispersion can provide information on the slope of the group-delay curve. This measurements can be used to initialize the profile without the need of other diagnostics[7]. Furthermore, direct sampling of distorted pulses can provide direct evidence of particular density fluctuations: away and close to the cutoff layer in the form of Bragg resonances[9] or wave-trapping, respectively[8].

Nearly 15 years after the last SPR publication[4], advances in digital electronics and mm-wave hardware have allowed limitations regarding spatial sampling and range resolution to be surmounted while increasing range precision by a factor of 4. This publication presents how a fast (65GSa/s, 25GHz analog bandwidth), multi-channel, arbitrary waveform generator (AWG) and a ×6 varactor multiplier can bring about flexibility in pulse carrier frequency, width, and repetition frequency. 25-point density profiles can be thus reconstructed with sub-cm spatial resolution and μs temporal sampling comparable with established continuous-wave reflectometry techniques[1]. Equally importantly, little work has been published[10] connecting short-pulse group-delay fluctuations with density fluctuations and establishing the potential of the technique as a fluctuation diagnostic.

The present article begins by presenting the hardware implementation in section II. It proceeds by presenting and comparing two approaches to measure pulse group-delays in section III. First data and preliminary results are presented in section IV followed by conclusions.

II. HARDWARE IMPLEMENTATION

Figure 1 shows both transmitter and receiver stages of TCV's SPR. The transmitter section produces pulses of 650-750ps full-width-at-half-max (FWHM) duration of arbitrary frequency inside the V-band (50-75GHz) by using 1-2s, 8.33-12.5GHz carrier, pulses from the Keysight M8195A AWG fed into a x6 varactor multiplier[11]. This frequency multiplier is found inside a transmitter/receiver (TX/RX) commercial off-the-shelf vector network analyzer (VNA) extension module built by Virginia Diodes Inc (VDI). Only the transmitter portion of the module is used and sketched in figure 1. The varactor multiplier has a non-linear response to input pulses leading to varying degrees of pulse compression and amplitude saturation. Nonetheless, thanks to the unique flexibility of fast AWGs, Gaussian output envelopes can be created by carefully controlling input pulse amplitude, duration, and phase. Figure 2 shows the envelopes of pulses of 650-750ps FWHM over the V-band measured with a fast zero-bias Schottky diode detector (>6GHz bandwidth WR15.OR4 1-16 from VDI) directly at the output of the varactor multiplier. The internal memory of the AWG allows launching up to 273 unique pulses at 16MHz repetition rate, which once played are looped inside a discharge. Sequencing capabilities, making use of the external memory, may allow over 10^6 unique pulses.

All integer frequencies in the V-band have been tested to provide output powers between -5 and -8dBm based on the sensitivity curves of the WR-15 diode. Figure 2 normalizes all pulse peak amplitudes and stacks them vertically for clarity purposes. The Tx pulses are transmitted to the plasma via TCV's diagnostic launcher. It consists of a quasioptical telescope, 6.5m of low-loss 65.3mm HE11 waveguide, a pair of fast miter-bend polarizers in HE11 waveguide, and a quasi-optical launcher antenna[12]. The telescope assembly was recently upgraded by replacing the smooth-walled U-band horn by a V-band corrugated Gaussian horn designed and built by Thomas Keating Ltd. Transmission-line insertion losses (IL) amount to ∼7.5dB. These were directly measured using a time-

domain-gated (TDG) vector-network analyzer (VNA). This figure does not include losses in the launcher antenna, which, based on Gaussian beam truncation due to mirror size, should theoretically remain under 0.3dB at 50GHz. Round-trip beam expansion and non-normal incidence at the cut-off layer may give rise to larger losses, independent of plasma reflection coefficients. The entire waveguide system is about 8.6m long. Thus, in order to avoid pulse ambiguity, pulses must be spaced by about 57ns which fixes the maximum unambiguous pulse repetition rate (PRR) at 17.5MHz. Pulse interleaving can be used to increase this PRR since the cut-off location ranges can be easily predicted. Assuming a separation of 10ns (15cm) between pulses, interleaving would allow for PRRs of up to 100MHz. Pulse interleaving is not demonstrated in this publication.

The receiver stage uses heterodyne detection for added sensitivity. Reflected pulses are coupled to a WR-15 VDI RX (receiver) module via a broadband directional hybrid coupler. A sensitive (0.1dB flatness) variable waveguide attenuator (STA-60dB-WR-15-D1 from Sage Millimeter) is used to limit the incoming power to avoid receiver saturation. The signal is then mixed with a local oscillator (LO). This LO is produced by multiplying a continuous-wave 8.33-12.5GHz signal provided by a second AWG channel synchronized with the pulse-producing channel. Given that this signal may contain analog distortions of up to -30dBc, it is first amplified (18dB gain, 2.2dB NF, FMAM1027) and then band-pass filtered (9.5-13GHz BPG7817A) to ensure a pure and strong LO is provided to the mixer. The resulting intermediate-frequency (IF) output was chosen at 8GHz, the largest frequency that permits receiving 0.5ns pulses inside the 10GHz mixer bandwidth limit. The IF pulse output is firstly amplified by a broadband (8-12GHz), low noise (2.2dB NF), high gain (38dB) amplifier (SLNA-120-38-22-SMA). The signal is then band-pass filtered at 8GHz (2GHz bandwidth BPF5620A) to remove the LO-bleed through and spurious mixer frequencies. This IF band-pass filter has a boxcar shape with -3dB and -30dB points at 6.91/9.14 and 6.75/9.31GHz, respectively (see exact shape in the appendix). Since the outgoing pulse widths are 700±50 ps, the reflected pulse bandwidth expected at 1.4±0.1GHz should comfortably sit inside the passband. However, as further discussed in appendix, pulse power outside the aggressive (50MHz/decade) boxcar shape leads to an increased pulse rise-time and ringing that distorts the pulse right-hand side.

The filtered pulse is then fed into a fast Schottky detector (302A from Krytar), which extracts the pulse envelope. Lastly, the pulse envelope is amplified by a low-noise (2.5dB NF) pulse amplifier (9kHz-3GHz SLNA-030-32-30-SMA). The amplified pulse is then low-pass-filtered (DC to 2.6GHz LPF8132A) to reduce noise as much as possible. A bias tee (Inmet 64671 8810SMF2-26) is used to reduce small DC offset voltages from the pulse amplifier to zero. The filtered pulse envelope is then sent to the timing circuits further described below. Figure 1 also shows AWG channels 3 and 4 producing pulse echo cancellation and synchronization signals. Their role is explained in section III B below. A SMA T is used to couple the pulse echo cancellation with the reflected signal. A 2-way combiner would be a better choice to ensure impedance matching, and it will be considered in future improvements to the diagnostic. All amplifiers and filters were procured from Fairview and UIY Microwave, respectively.

III. TIMING CIRCUITS

A. Requirements

Assuming the outer 20% of the confined TCV plasma (∼5cm) to feature a parabolic density profile, reconstructing a 20 point density profile requires a 2.5mm range resolution. Such a resolution in vacuum corresponds to requiring the timing circuits to discern pulse round-trip group-delays with a 17ps maximum error. In order to obtain a 20-point profile measurement with a competitive[1] 1.25μs temporal resolution, a pulse repetition rate (PRR) of at least 16MHz is required. At these pulse repetition rates, the timing circuits should be capable of recording $32{\cdot}10^6$ group-delays to cover the full 2 seconds of the standard TCV discharge. As seen above in section II, unambiguous pulse repetition rates with TCV's diagnostic launcher system comfortably allow for a 16MHz PRR. Pulse interleaving has the potential to enhance the temporal resolution of a 20 point profile down to 0.2 μs.

B. Traditional analog approach

Traditionally, short and ultra-short pulse reflectometers have used a combination of a constant fraction discriminator (CFD), a time-to-amplitude converter (TAC), and an analog to digital converter (ADC) to measure group-delays. All these elements have been identified in the commercial SPC-150NX timing module from Becker and Hickl GmbH shown in figure 3[13].

Since the reflected power from the plasma can vary as a function of frequency and shot conditions, the CFD's function is to trigger the reception of a pulse irrespective of its incoming amplitude. After receiving a pulse, the CFD outputs a TTL signal that is fed into the *start* input of a TAC which also receives a *stop* (SYNC in figure 3) pulse directly from the AWG (Ch 4 in figure 1). The output voltage of the TAC is proportional to the time difference between the start and stop signals. This voltage is digitized by a 14-bit ADC. The time difference can be measured with a resolution of maximum 450fs. At this resolution, the temporal range of measurements is limited to 1.5ns, which accommodates group-delays from targets up to 22cm apart in vacuum (well over the 5cm requirement). Altogether, the module is capable of recording

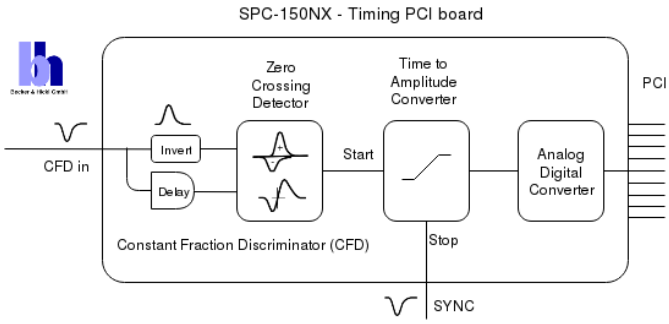

FIG. 3: SPC-150NX schematic diagram[13]. Reproduced with permission from Becker and Hickl GmbH.

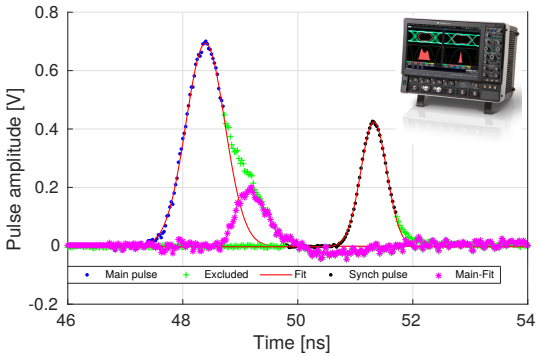

FIG. 4: Sample least-squares fit of reflected and synchronization pulses. R^2=0.998.

time differences with an electrical time resolution of 1.6ps root-mean-square (RMS). In addition, the module may be operated at a count rate of up to 10MHz. It may acquire up to 2×10^6 events, which at 10MHz corresponds precisely to the standard TCV discharge duration. Unfortunately, given that the AWG-generated LO must be defined in multiples of 128 samples, the maximum pulse repetition rate achieved under 10MHz has been 8.33MHz, a factor of 2 under the 16MHz requirement.

Figure 1 shows an AWG channel acting as an echo cancellation channel. This signal is required to actively cancel reflections along the signal path to avoid premature triggering of the CFD. These spurious reflections come from the limited directivity of the hybrid coupler, reflection coefficients of waveguide filters[12], and, most importantly, from the vacuum window at the entrance of the launcher antenna. Reflections from the coupler and filters remain under -16dB, but the vacuum window reflections may be as large as -5dB. All reflections along the line were firstly sampled for each discrete frequency using a fast oscilloscope (see section III C below). The recorded traces were inverted, played back by the AWG, amplified, and time-shifted so they coincide with the reflections. Echo pulses of up to 1.2V are thus reduced to less than 100mV (well under the 200mV CFD walk limit). Imperfections in the cancellation technique do not affect the group-delay measurements since the signal travels at least 2m to and from the cutoff away from the vacuum window: over 10ns separate the two signals in time.

C. Direct sampling approach

A newly tested approach to quantifying group-delays is to directly sample the pulse envelope with a fast analog to digital converter (ADC). A fast (45GSa/s), 8-bit, 13GHz analog bandwidth oscilloscope (LeCroy 813Zi-B) is used for this purpose. A sample reflected pulse from the HE11 mirror is shown in figure 4. A Gaussian function is fit via least-squares. Unfortunately, the leftover Gaussian pulse power outside the IF filter pass-band produces ringing in the form of small-amplitude pulses following the main pulse. These small pulses interfere and distort the right-hand side of the main reflected pulse. Figure 4 shows direct evidence of these phenomena in the magenta waveform resulting from subtracting the pulse raw data from its Gaussian fit. More details are presented in the appendix. As a result, the Gaussian fit of the main pulse ignores 70% of the right portion of the pulse. The synchronization pulse coming straight from the AWG is also shown; it is fit ignoring only the outer 20% of the right portion of the pulse. These rejection percentages were empirically chosen to maximize the number of points taken into account in the Gaussian fit, ignoring any departures from this functional form. Ringing pulses do not affect the performance of the analog SPC-150Nx circuits since only the pulse rising time is used by the CFD to trigger the TAC.

Direct sampling has the immense advantage of storing the reflected pulses; future post-processing routines can re-interpret the data. Another advantage is that the fits return not only the time difference between input and SYNC pulses but also pulse envelope amplitude and width. Furthermore, this timing approach does not require active pulse cancellation. Lastly, the PRR can easily exceed the 16MHz requirement via pulse interleaving.

However, this technique does feature a few drawbacks. Loading large ADC traces and fitting individual pulses to access group-delays requires more computing post-shot computing power. Yet, modern computers allow hundreds of fits within a few minutes. Perhaps the biggest disadvantage is the large memory requirement. At 45GSa/s, the limited oscilloscope memory of 32 mega samples allows a pulse train of only 0.7ms to be acquired. Multiple triggering may allow sampling of up to 8x250s instants during a shot. Nonetheless, such small sampling time remains impractical for routine density profile measurements.

D. Comparing the two pulse-timing techniques

As outlined in section III A, the ultimate group-delay uncertainty is composed of three contributions: intrinsic

hardware precision, random noise, and changing input pulse amplitude errors.

In the SPC-150Nx case, the first contribution comes from the intrinsic minimal electrical time resolution of the timing hardware at 1.6ps. In the direct sampling case, the intrinsic hardware errors come from the ADC clock jitter and/or from the limited sampling frequency. The sampling clock RMS jitter of the LeCroy 813Zi-B is 0.15ps for one channel and up to 0.33ps between channels. Another source of intrinsic hardware error may be the finite sampling period of the scope at a minimum of 22ps, although a good fit to the Gaussian envelope may achieve group-delay resolutions better than this sampling interval[14]. To test this assertion, 166 pairs of 700ps FWHM Gaussian pulses were produced by the AWG and fed directly into two separate scope channels. The time difference between them was normally distributed with a SD of 1.15ps. Thus, both techniques feature intrinsic hardware errors under 1.6ps.

The second source of uncertainty comes from unavoidable thermal noise in the mixer and amplifiers, which translates into fluctuations in the pulse envelope fed to the timing circuits and into group-delay errors at constant input power. This contribution can be estimated by looking at the standard deviation (SD) of group-delay measurements against a static target. Irregularities in the output power of the AWG, the varactor multiplier, and the receiver mixer as well as non-flat transmission curves of filters and polarizers may cause the effect of thermal noise to change with frequency. An HE11-waveguide mirror at the entrance of the launcher antenna has been used to measure these changes. Reflections from this mirror take into account the response of all components except for the vacuum window and the launcher which are inaccessible when TCV is under vacuum. Simulating a plasma reflection coefficient (S11) of -10dB using the variable attenuator in figure 1 with respect to a perfect mirror yields a mean SD of 8ps with the SPC-150NX module and 7ps with the direct sampling technique. Figure 5 shows how these SDs change over the V-band for a -25dB attenuation, corresponding to the lowest allowed amplitude of 200mVpk (see table I). Group-delay data against this static mirror shows excellent agreement with the normal distribution.

The third source of uncertainty comes from changing input pulse power. In the SPC-150Nx case, CFDs are meant to lock equally to pulses of varying amplitude, but they feature a non-zero variation in the locking time as a function of input pulse amplitude known as *time-slewing* or CFD *walk*. In the direct sampling case, since a Gaussian fit adapts specifically to the incoming amplitude, this approach should intuitively prove to be more resilient. However, the limited ADC resolution (8-bits) and fixed ADC gain in the presence of noise makes the fit of low-amplitude pulses less reliable. The adjusted coefficient of determination R^2 is used to judge goodness of the Gaussian fit. Only pulses with $R^2 > 0.985$ are counted since allowing lower R^2 fits results in large group-delay variations above the 17ps requirement.

Pulse type	**SPC-150Nx locking error [ps] 10^6 counts**	**Direct Sampling locking error [ps] 10^3 counts**
AWG clean 500mVpk	1.6	1.15
Amp. change 500-35mVpk	8 ZC=5mV	5 R^2=0.985
<mmw> noisy 500mVpk -20dB S11	9	8
Amp. change 920-200mVpk -15/-25dB S11	13 ZC=24mV	10 R^2=0.985
Total	17	14

TABLE I: Group-delay precision comparison of both timing techniques.

In order to quantify this contribution, firstly, low-noise 700ps-FWHM Gaussian pulses from the AWG were used to characterize the fundamental response of each timing technique in the lowest possible noise conditions. The clean pulse peak amplitude was varied between 500 and 35mV. A CFD walk of up to 8ps was recorded with the SPC-150Nx using a zero-crossing (ZC) point[13] of 5mV. The direct sampling approach showed an equivalent walk of up to 5ps. Then, the HE11 mirror in combination with the variable attenuator were used to quantify walk errors including all noise sources and power variations over the V-band. Peak pulse amplitude was varied between 920 and 200mV, simulating a 10dB power change in the plasma. Using a ZC point of 24mV, the SPC-150Nx walked by 13ps in average. The direct sampling walked by 10ps in average. Table I and figure 5 show how each timing technique responded to changing input amplitudes.

The total timing error is estimated by adding in quadrature all three error sources presented above and results in a mean over frequency of 17ps for the SPC150-NX and 14ps for the direct sampling technique. Figure 5 shows the individual error contributions (omitting the intrinsic hardware error, which is negligible) at discrete frequencies across the V-band. Unfortunately, frequencies 50, 64, and 73-75GHz did not provide a strong signal in the receiver and resulted in final errors much larger than the 17ps requirement. The power-level drop is localized in the Rx module since these frequencies were found to produce a good output signal in the diode tests shown in figure 2.

Since triggering of pulses of amplitudes under 200mV would lead to unacceptably high CFD walk, the SPC-150Nx is programmed to ignore pulses under 200mVpk. The direct sampling technique stores all pulses regardless of incoming amplitude. However, the current fitting routine accepts only pulses fit with a $R^2 > 0.985$ which also limits amplitudes above 190mVpk. This threshold requires the launcher-plasma reflection coefficient (S11)

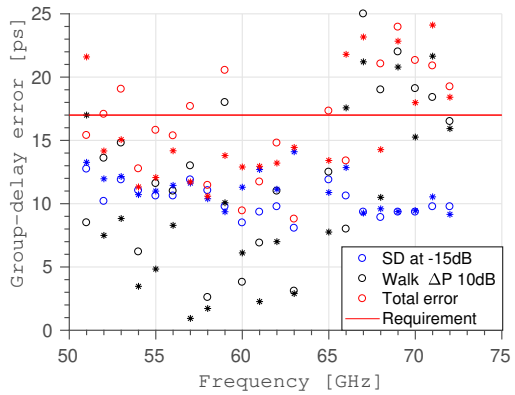

FIG. 5: Realistic estimation of the total group-delay error of the SPC-150Nx (∘) and direct sampling (∗) techniques in the V-band considering 10dB power variations in reflected power.

of every pulse to be above -25dB so the it can be successfully counted. Note that turbulent plasma S11 may be as low as -45dB due to 2D-scattering[15], hence, it is expected that varying amounts of launched pulses may not be counted in the receiver depending on the plasma conditions and alignment at the cut-off layer (see section IV A).

E. Pulse amplitude and width reflected from lossy static mirror

Direct sampling fits provide not only group-delays but also pulse envelope amplitude and width. Following the clean and noisy definitions in table I, table II shows the amplitude and width evolution with power. Firstly, the amplitude estimates seem robust to power changes. Even in the presence of full-system noise, the amplitude SD stays under 1%. However, the width estimate seems to vary by as much as 4%in low-amplitude pulses. Pulse width is also seen to significantly decrease (beyond the SD) as the pulse amplitude is decreased when the full mmw system hardware is used. This may be due to the Schottky diode's impedance variations as it departs from the square-law region with high input power. Nonetheless, given the careful characterization of group-delay errors above, these power-driven pulse-width variations do not affect the group-delay accuracy as quantified. However, pulse width variations caused by pulse dispersion in the plasma can affect group-delay determination in a fashion not characterized in this study. In principle, the AWG's flexibility can be used to vary the launched pulse width, but such calibration has not been performed yet.

Amplitude		**Width**	
mean [mV]	SD [mV]	mean [ps]	SD [ps]
AWG clean 500	1.2	717	3
35	1	696	35
<mmw> noisy 920	13	783	10
528	11	748	11
219	7	720	24

TABLE II: Pulse peak amplitude and width evolution at power variation extremes against static mirror.

IV. RESULTS AND DISCUSSIONS

Both timing techniques presented in this article were used in plasma discharges. Comparing group delays between identical L-mode discharges 61831 and 62642 revealed that both techniques measured group-delay differences between pulses of carriers 51 and 58GHz within 6ps. Given the overly small sampling duration available in the current direct sampling implementation, the SPC-150Nx timing solution was the only practical option to extract physically useful group-delay data as shown in the section IV B below. Before focusing entirely on the group-delay results, the next section presents the variations in pulse amplitude and width observed in the plasma with the direct sampling technique.

A. Pulse amplitude and width reflected from L-mode plasmas

The direct digital sampling technique was used to measure about 2700 pulses reflected from L-mode plasma 62642 with frequencies 51-57GHz. After fitting, about 65% of recorded pulses featured R^2 above 0.985, which added up to 250 pulses per frequency. Statistical analysis of these well-fit pulse amplitudes and widths are shown in table III.

Quantity	**mean**	**SD**	**max**	**min**	**skewness**
Amplitude [mV]	550	220	1120	190	0.48
Width [ps]	780	70	1140	610	1.02

TABLE III: Pulse peak amplitude and FWHM statistics during L-mode plasma 62650. Table presents averages of frequencies 51-57GHz for 333μs at 0.7s (ρ_ψ 0.9-0.83. $k_\perp$ <50m^{-1}).

Raw pulse amplitudes were found to vary strongly, between 1.2V and the noise floor at the mV level. Hence, raw power variations may easily exceed 40dB, in agreement with power modulations extremes estimated by Conway[15]. Fits with adjusted R^2 >0.985 allow only pulses of Gaussian shape and amplitudes above 190mV to be meaningfully studied. Enforcing this double filter, average amplitudes in L-mode sat at an average 550mV

with a SD of 220mV. Notice that the amplitude scatter in a L-mode plasma is an order of magnitude above the amplitude scatter caused by noise in the mmw circuits presented in table II.

Reflected pulse widths can also vary strongly. There are cases where the reflected pulse is not a single pulse. Considering only single-Gaussian reflections with R^2 >0.985 fits that work only for Gaussian single pulses, pulse widths can range from 1.12ns down to 0.61ns showing experimental evidence of pulse dispersion[7]. The minimum pulse width of 610ps, safely away from fit uncertainty under 30ps, shows that the plasma can shrink the pulse width; this is an unexpected result. Considering that the average pulse amplitude recorded was 550mV, the average pulse width was expected at about 748±11ps from tests against a mirror. However, the average pulse width reflected from the plasma is found to be 780ps with a SD of 70ps. This SD is due solely to plasma-induced pulse width variations since pulse width changes due to pulse amplitude variations have been taken off the SD using the calibration data shown in table II. The skewness of width changes is strongly positive, indicating a higher tendency of reflected pulses to feature a larger width than average.

Pulse width fluctuations as quantified above can affect the group-delay precision of both timing techniques. In the direct digital sampling approach, a good Gaussian fit should intuitively allow for an accurate determination of a group-delay if the dispersed pulse maintains a good Gaussian shape and amplitude. Also since amplitude, width, and group-delay are recorded, severely dispersed pulses can be safely discarded in averages attempting a density-profile reconstruction from group-delay data. Unfortunately, however, the analog SPC-150Nx module is currently blind to pulse width changes. Analog measurement of rising and falling edges is in principle possible [6]. The effect of varying pulse width on the SPC-150Nx group-delay precision has not been quantified. However, a first-order guess can add half of the standard deviation of pulse width measurements (70ps) to the group-delay uncertainty. Only one-half of this scatter is taken because only the rising portion of the pulse is used to trigger the pulse arrival in the CFD. The average L-mode plasma group-delay error then becomes 39ps by adding in quadrature 35ps and the 17ps error quantified above. No direct-sampling data was available from H-mode plasmas at the writing of this article, but dispersion is expected to be lower based on the observed reduced scatter of group-delay data as shown in the section IV B below.

It must be noted that because the pulse/IF-filter shape mismatch, the pulse width results presented here can only be considered preliminary and at-best only indicative of true plasma-induced pulse width changes. As fully addressed in the appendix, the amount of shape mismatch has an effect on the pulse rise-time being measured by the direct-sampling Gaussian fit above.

B. Group-delay statistics from L and H-mode plasmas

The data presented here onwards corresponds to group-delays measured with the SPC-150Nx analog timing module. When moving from the static mirror to the plasma target, the first observable feature was that the scatter of the raw group-delay data changed significantly as a function of plasma conditions. Three factors may affect these group-delay fluctuations: variations in returned pulse power, signal to noise (SNR) variations, and physical changes to the pulse group-delay or shape. As presented in section III B, electrical noise and CFD walk contribution at the allowed pulse amplitude ranges (10dB) can amount up to 17ps (in average) at power extremes. Tests against the HE11 mirror *during* a discharge revealed negligible increased electrical noise interference in the measurement: identical group-delays scatter was measured during and after a shot. Therefore, changes in the raw group-delay histograms for pulses at 58GHz beyond a normal distribution with a 14ps SD are due to plasma-driven changes to the group-delay and/or width. Figure 6 shows the normalized histograms of frequency 58GHz acquired for 100ms at 8.33MHz PRR against the HE11 mirror and during the L-mode and (ELM-free) H-mode phases of discharge 62633 (I_P 360kA, δ=+0.44, Z=23cm, I_P driven H-mode). The maximum of the histograms has been shifted to an arbitrary zero group-delay so the shape of the individual distributions can be best compared. The O-mode polarization ensures that changes in group-delay are entirely due to fluctuations in the electron density.

Basic statistical moments of the raw group-delay data can be seen in table IV. L-mode plasmas show a 10-fold increase in the scatter versus a static mirror. Pulse width changes caused by dispersion in the plasma are not taken into account by the SPC-150Nx, but as presented in section IV A these may contribute to an increased scatter of up to 35ps. Altogether, a L-mode plasma do seem to fluctuate with a 2.5-fold increase over the noise floor.

H-mode plasmas show only a slight increase in group-delay scatter versus the mirror total error at 14ps (for 58GHz). The marked decrease in group-delay fluctuations is consistent with the well-known fact that density fluctuations are suppressed in the edge of H vs L-mode plasmas due to turbulence decorrelation by shear-flow. The reduction is also consistent with analytical formulas presented by Fanack et al.[16], which present the level of phase fluctuations of a single frequency CW reflectometer are not only proportional to the density fluctuation level but also to the square root of the density gradient length $\Delta\phi_{\max} \propto \delta n_0 \sqrt{L_n/k_f}$ (where $L_n = n_e/(dn_e/dr)$ and k_f is the fluctuation wavenumber). This analytical formula applies to large wavelength fluctuations ($k_f \ll k_o$) and small fluctuations where the *spatial* regime of Bragg scattering applies ($2k_{\text{Airy}} < k_f < 2k_o$[16]). Also, the increased gradients are less likely to cause pulse width dispersion, which may also reduce the group-delay scatter. The increased group-delay scatter in the plasma over the

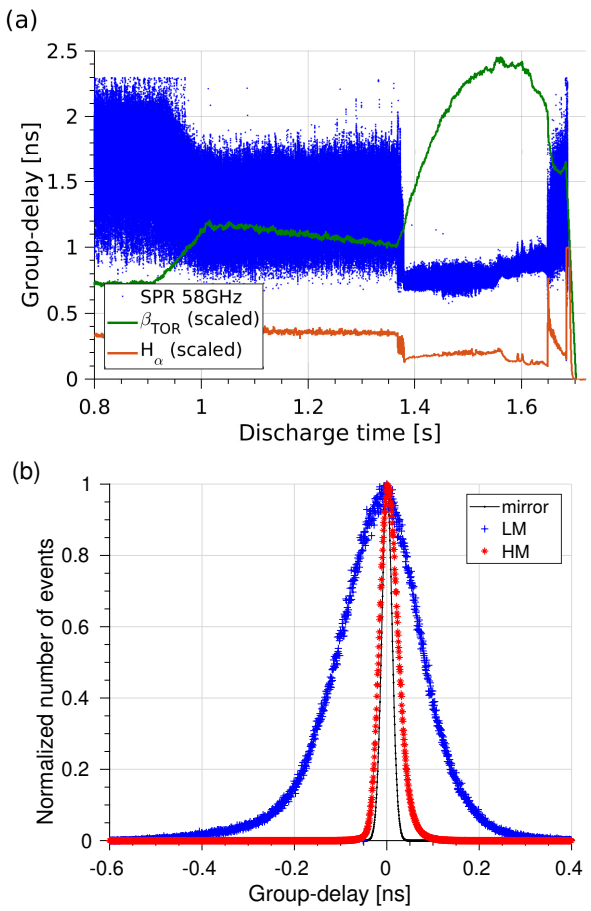

FIG. 6: (a) Raw group-delay data for frequency 58GHz during shot 62633. (b) Histograms of group-delay data during L-mode (1.15-1.25s), and H-mode (1.4-1.5s) phases compared with against a mirror. Pulse return rates are 93 and 96% for L-mode and H-mode sections respectively. Cut-off location (ρ_ψ) and perpendicular wavenumber $k_\perp$ were found to be 0.91 and 58m^{-1} during the L-mode and 0.99 and 23m^{-1} H-mode phases using the PrefGeom ray-tracing code.

Target	Stdev[ps]	Skewness	E. Kurtosis
Mirror -10dB	11.2	0.004	0.02
L-mode t=1.15-1.25	109	-0.52	1.73
H-mode t=1.4-1.5	22	0.65	1.95

TABLE IV: Basic moment analysis of raw group-delay data during shot 62633.

mirror has also been reported by Heijnen[3] (180ps) and Shevchenko[17] (147ps).

Skewness is also seen to change as a function of plasma conditions. It is seen to transition from negative to positive going from L to H-mode. Excess kurtosis exists in both L and H-mode quantifying that the group-delay statistics is beyond normal in both cases, suggesting possible burstiness. It can be expected that rich physics information could be extracted from these findings with the aid of synthetic modeling of pulse reflection in the presence of realistic tokamak plasma density fluctuations.

C. Frequency spectrum of group-delay data

Conventional continuous-wave fluctuation reflectometers have been able to unequivocally identify macroscopic MHD density fluctuations from the power spectral density (PSD) of phase variations[18]. Studying the PSD of raw group-delay data has revealed a similar potential. Sawtooth oscillations with a period of about 320Hz have been clearly observed as large variations in the group delays at a pulse frequency of 66GHz during shot 60491, which found a cutoff at about $\rho_\psi = 0.76\pm0.01$. TCV's far-infrared interferometer chord number 4, which vertically integrates at the same major radius as where the cut-off is found (R=0.972m), shows the same oscillation frequency. In addition to these low-frequency macroscopic modes, the PSD of group-delay data has shown evidence of a ∼40kHz quasi-coherent mode in the edge of ELM-free H-mode plasmas as shown in figure 7. These modes have been also observed by TCV's magnetic pick-up coil arrays[19]. TCV's magnetic analysis routines[2021] have been used to identify a mixture of even toroidal mode numbers with dominant n=0 and n=2 propagating in the counter-current direction. Poloidal arrays hinted at a m=0 mode number.

D. Density profile measurement

The fast miter bend polarizers installed in TCV's diagnostic launcher[12] allow the instrument to operate in both O and X-mode polarizations. V-band frequencies encounter cut-offs at 3-7 and 0.8-4 $\times10^{19}$ m^{-3} in O and X-mode, respectively, during typical L-mode TCV discharges. Prior to attempting measurements of density profiles, individual frequencies are calibrated against the lossy-mirror target at the entrance of the launcher modeling average plasma losses through a fixed -15dB attenuation. Their individual group-delays are measured and then time-delayed so that all frequencies give the same group-delay within 1ps against the static target. This step is necessary to discard group-delay variations over frequency produced by the mm-wave and transmission-line hardware. The TAC/ADC linearity of the SPC-150Nx was confirmed by artificially delaying the synchronization pulse over the entire measurement range of 1.5ns. The last calibration step consists of applying a correction curve for the pulse group-delay changes through the vacuum window. The quartz interface acts as a Fabry-Perot interferometer with varying amounts of absorption and reflection over the V-band resulting in variable group-delays of as much as 30ps. These group-delay variations were quantified on an optical table using

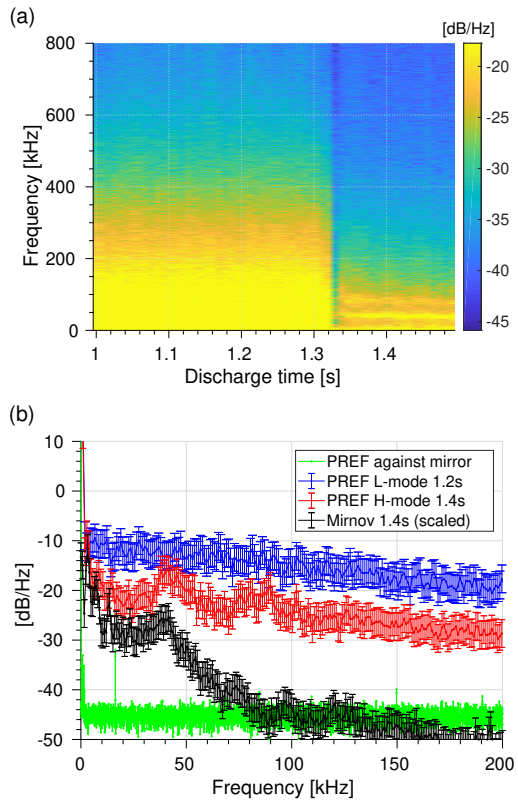

FIG. 7: (a) Spectrogram of SPR raw group-delay data of freq. 51GHz over L-H transition during shot 61834. (b) Snap shots of SPR PSD at specific times during L (ρ_ψ=0.97, $k_\perp < 13$ m^{-1}) and H-mode (ρ_ψ=1.0, $k_\perp <$ 45m^{-1}) sections compared with PSD of SPR against mirror and PSD from Mirnov coild No.77 in sector 13. Time windows of 10ms taken for all snaps. Pulse-return-rates are above 85%.

Gaussian beam antennas and TDG VNA measurements. These were later confirmed during a vacuum opening of TCV with a mirror installed inside the vessel facing the launcher antenna.

1. O-mode density profiles

Profile measurements require a plasma whose cutoff layers are normal to the beam's wave-vector over a good portion of the V-band range. Once group-delays have been measured for a number of frequencies, the well-known Abel transform can be applied in O-mode polarization to obtain a density profile[22]. Unfortunately, all reflectometry implementations feature the limitation of having group-delay information only above a non-zero frequency (in this case 50GHz). Information regarding the $\partial\phi/\partial f$ curve below the lowest frequency must be obtained from other diagnostics and/or by assuming a particular model[23].

In our case, group-delay initialization is obtained using the 2D ray-tracing routine PrefGeom. This code is presented in a recent publication[12]. It uses TS data inside the LCFS (and beyond when available) and features a realistic double-decaying exponential scrape-off-layer (SOL) density profile based on recent measurements[24]. The SOL profile extent is defined from the LIUQE magnetic reconstruction as the distance between the LCFS and the vessel wall (outer gap). Vessel volume beyond this point is termed the wall shadow[25], and it is expected to feature very low plasma densities, rapidly decreasing to zero after the far SOL. Thus, the wall-shadow volume traversed by the mmw beam is treated as vacuum. PrefGeom is used to identify the cut-off frequency at the transition between the far SOL and the wall-shadow, usually between 10 and 20GHz in O-mode. Then, taking 20 steps from this frequency up to 50GHz, ray-tracing is performed to obtain the cut-off locations as a function of frequency. The Abel transform is then numerically inverted to find the group-delay curve between 15/25 and 50GHz. The advantage of this approach is that the curve is inferred from recent published average SOL density measurements[24] and not models[23]. The disadvantage is that when the 50GHz cut-off is found above the LCFS, the initialization $\partial\phi/\partial f$ curve is only available on the TS 60Hz period.

Figure 8 shows the density profile evolution during a L-H mode transition recorded with 11 frequencies during shot 62744. Pulse return rates are above 82% during L-mode and above 98% during H-mode. The frequency span 50-61GHz was chosen because higher frequencies featured $k_\perp$ >50m^{-1} and hence could not be sampled at perpendicular incidence at the same chosen launcher poloidal angle of 29°. The group-delay data in 8a and 8b was averaged over 8.75μs to produce each profile, which averages about 5 pulses in each frequency. SPR density error bars come from the finite width of the 700ps FWHM Gaussian pulse in the frequency domain: ∼0.61GHz SD. The ρ_ψ error bars come from the spread in the group delays (SD divided by the square-root of number of pulses) added in quadrature with the 40ps hardware error presented in section IV A.

There are many sources of uncertainty that are extrenous to the SPR instrument. Figure 8b shows the Airy width[26][pg.90] which is an estimate of the cut-off layer width. The blue and green colors refer to the L and H-mode instants, respectively. Also, a $\Delta\rho_\psi$ error is shown. It comes from the finite mmw beam size at the cut-off which introduces uncertainty regarding the ρ_ψ location of the first cut-off frequency. It was estimated using 3-point ray-tracing[12]. Lastly, the effects of TS density magnitude and position errors are also included in figure 8b. The TS magnitude error during this discharge is found to be 3%. The density profile used for ray-tracing and profile initialization is varied within this range to estimate the effect on the location of the first frequency cut-off. TS position errors (assuming an accurate Z-position calibration) are dominated by LIUQE plasma position errors. Based on recent results by Dellaferrera[27] from covariance analysis

of L-mode shots in TCV, a vertical plasma position error of 3mm can lead to a $\Delta\rho_\psi$ of 0.005. SPR data points without error bars come from the initialization procedure. Uncertainty in the density reconstruction due to changes to the SOL profile has not been taken into account in this publication.

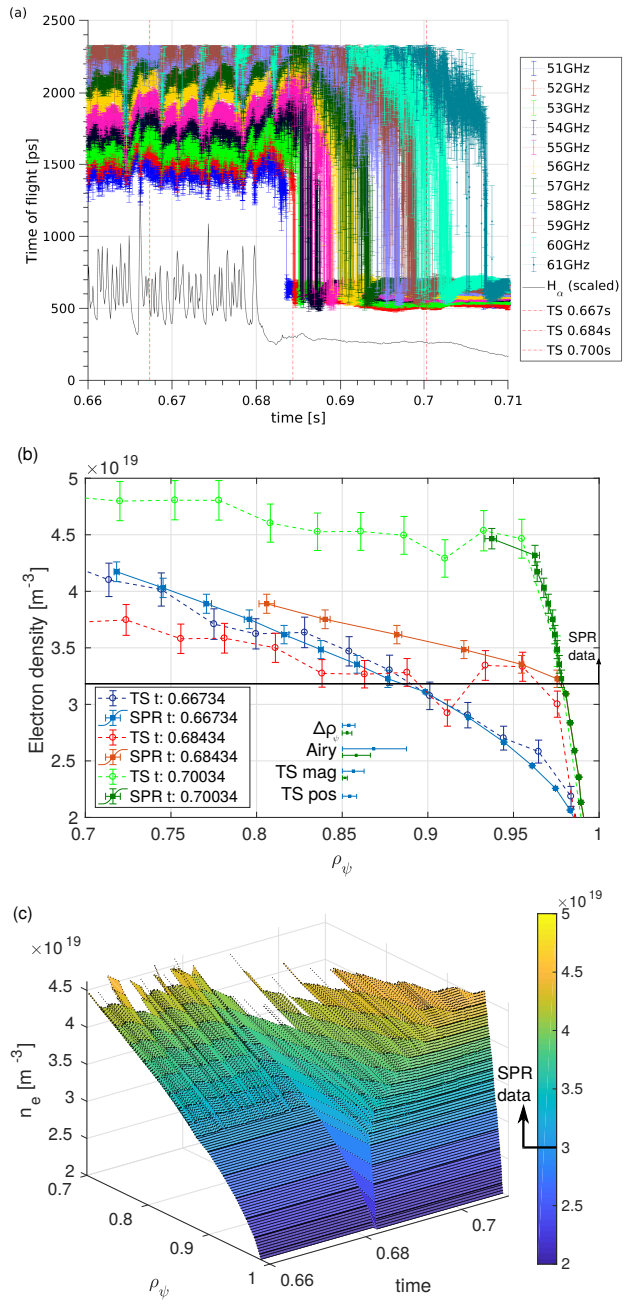

FIG. 8: SPR density profile in O-mode during an L-H-mode transition in shot 62744. 8.75μs averaging is applied to all sub-figures. (a) SPR raw group-delay data. (b) Comparison with TS profiles at TS sampling instants. (c) Density profile time evolution.

2. X-mode density profiles

The Bottolier-Curtet algorithm[28] can be used to transform phase differences between frequencies into distances to a cut-off layer. Knowledge of the magnetic reconstruction allows this information to be transformed into density profile over ρ_ψ. SPR group-delay measurements over frequency are transformed into phase change over frequency through trapezoidal numerical integration. The magnetic field is obtained from the LIUQE reconstruction inside the Psi-toolbox framework. The initialization problem is also present in this polarization. Unfortunately, since the current SPR implementation features frequencies in the V-band, it was not possible to use lower frequencies to find out experimentally the shape of the density profile under 50GHz. Instead, the measured TS density profile and the Vianello et al.[24] average SOL profile is used as in the O-mode inversion above. These profiles provide the shape of the refractive index and the position of the first cutoff layer.

Since the TS profiles are available only at 16ms intervals and given that SPR provides measurements of group-delays in the micro second level, a special initialization procedure is proposed. At the very instant of the TS measurement, PrefGeom is used to estimate the ideal group-delay for the lowest sampling frequency. Since precise magnetic reconstruction data and very good estimates of confined and SOL densities are available at that instant, the round-trip group-delay between the shadow and 50GHz cut-off is estimated. The measured first-frequency SPR group-delay is then scaled to fit the model above at the TS measurement instant. Any future changes to the measured lowest-frequency group-delay indicate a change to the integrated refractive index above. This change can be due to changes to the magnetic reconstruction and/or the density profile. If the first measured group-delay has changed beyond the SPR uncertainty including dispersion effects at 40ps (6mm in vacuum), then the updated LIUQE reconstruction is firstly fed into PrefGeom to calculate an updated group-delay. If the new magnetic reconstruction cannot account for the change in group-delay, then the TS density profile is scaled iteratively until the modeled group-delay matches the measured group-delay within uncertainty. This approach allows the evolution of the first reflection point of SPR profiles to evolve inside the TS 16ms periods. Figure 9b shows how this first reflection point moved using the above-mentioned approach between 0.2 and 0.217s in discharge 60928. Figure 9 shows an example of using this approach to infer the evolution of the density profile during the plasma startup phase of shot 60928. Note that without knowledge of the physical location nor the profile shape of the next TS period, the algorithm arrives at excellent agreement with the TS sampling point at t=0.21734. Given the large averaging used to avoid excessive data points in this example, the SPR profiles look rather smooth in contrast with the TS profiles which include the fluctuations present at the sampling instant.

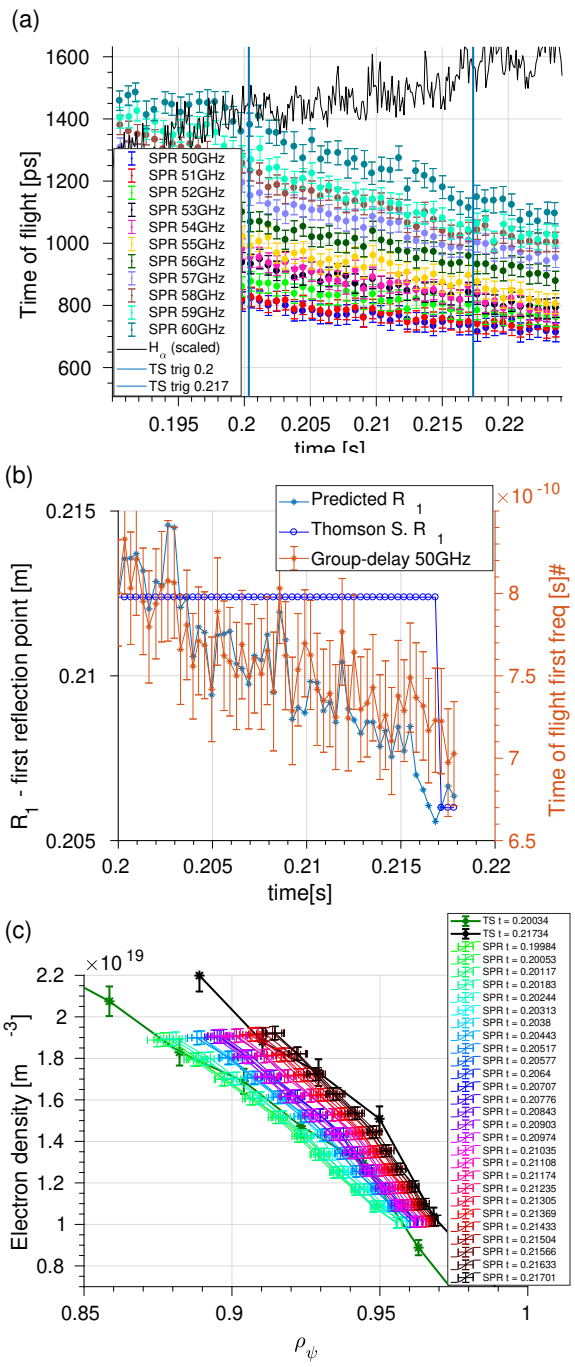

FIG. 9: Density profile evolution during plasma startup in shot 60928 using X-mode polarization. (a) Raw group-delay with 500μs averaging (b) Evolution of first reflection point (c) Comparison with TS.

The error bars in figure 9c are calculated using the error propagation formula. Group-delay uncertainty (adding 40ps of experimental uncertainty in quadrature with the SD of group-delays in the averaging window) is transformed into phase difference uncertainty by error-propagation through the trapezoidal integration formula assuming exact frequency steps guaranteed by the exact pulse carrier frequency steps produced by the AWG. In the Bottolier-Curtet inversion procedure, the width of pulses in the frequency domain (Gaussian SD) are taken as a source of uncertainty as well and propagated together with phase difference errors.

V. FUTURE PLANS

The direct sampling approach promises an exciting future for the diagnostic. SPC has recently purchased a fast sampling system from Guzik (ADP7104 10-bit 32GSa/s) with a memory of up to 64GBytes. This sampling system, featuring a 10GHz analog bandwidth, will allow direct sampling of the mixer output from the Rx module for over 1.5 seconds. Digital analysis of this data should allow measurements of phase and possibly Doppler shifts, in addition to the group-delay, amplitude, and width demonstrated here. Without a hardware IF filter in the receiver, this system would also allow the output pulse width to change during a shot, allowing pulse dispersion studies[7] and completely removing the smoothing bandwidth limitation of analog pulse detection. Lastly, a direct digital sampling system should allow for faster pulse repetition frequencies by interleaving pulses, optimistically increasing the time resolution down to 0.2μs.

Profile reconstruction methods presented here use the Abel inversion for O-mode and the Bottolier-Curtet method for X-mode. The latter assumes a linear refractive index shape in each integration step, which can lead to inaccurate profile inversions. More adequate functional representations of the refractive index have been recently introduced by Morales et al. [29] and Shelukhin et al.[30] which have the potential to improve the accuracy of the recovered profile.

Important hardware improvements for future work can begin by changing the shape/bandwidth of the IF filter to avoid pulse ringing and changes to the rise-time. The SMA 'T' connecting the echo-cancellation channel to the timing-circuit input can be replaced by a combiner with better impedance matching properties.

VI. CONCLUSIONS

This article has described the technical details and first data of a newly developed broadband short (ns-scale) pulse reflectometer on the TCV tokamak. The instrument can access both equilibrium density profiles and density fluctuation information with sub-cm spatial resolution and micro-second time resolution. The output polarization freedom allows coverage of 3-7 and 0.8-4 10^{19} m^{-3} densities in O and X-mode, respectively. Short pulses in the V-band have been produced by using a fast AWG and x6 varactor multipliers. The group-delay of these pulses has been measured down to 17ps resolution using both analog and direct sampling techniques against a mirror including 10dB power variations. Di-

rect sampling has allowed measurements of pulse width variations showing that while dispersion does occur, in average, pulse widths increase only by 4%. The scatter of measured pulse widths motivates an increase in the analog-timing group-delay uncertainty from 17 to 40ps in a plasma target, which decreases the vacuum group-delay range precision from 2.5 to 6mm. It has been observed that pulse group-delays reflected from L-mode plasmas feature fluctuations in the 100ps level illustrating plasma density fluctuations. When aiming at mean profile reconstructions, time averaging can be used to reduce these fluctuations at the expense of temporal resolution.

Previous limitations of SPR systems[5] regarding spatial sampling and smoothing bandwidths have been fundamentally removed in this implementation. The 2GHz IF filter fixes the pulse bandwidth in hardware. However, the flexibility regarding pulse carrier frequency should allow for an effective arbitrary smoothing bandwidth where subsequent pulses can sample arbitrarily small steps in frequency. Integer steps have been demonstrated in this first publication.

ACKNOWLEDGMENTS

Vladislav Scheslavskiy from B&H is thankfully acknowledged for prompt feedback and helpful discussions regarding the performance parameters of the SPC-150Nx module. Jeffrey Hesler and Steven Durant from VDI are thankfully acknowledged for prompt feedback and helpful discussions regarding the performance parameters of the VNA extension modules. Stefano Alberti and Timothy Goodman are thankfully acknowledged for helpful discussions and for facilitating access to low-power mmw hardware at SPC. Cedric Tsui is gratefully acknowledged for helpful discussions regarding SOL density profiles. This work is partially supported by Requip grant (No. 206021-150707) of the Swiss National Science Foundation and by the Helmholtz Virtual Institute on Plasma Dynamical Processes and Turbulence Studies using Advanced Microwave Diagnostics. This work has been carried out within the framework of the EUROfusion Consortium and has received funding from the Euratom research and training programme 2014-2018 and 2019-2020 under grant agreement No. 633053. The views and opinions expressed herein do not necessarily reflect those of the European Commission.

Appendix: Pulse ringing

The current section briefly describes the source of ringing pulses observed in figure 4: the shape mismatch between pulse spectrum and the IF filter amplitude response. Figure 10a shows the fourier spectrum of a 650ps pulse (the shortest pulse duration expected from WR-15 diode measurements presented in figure 2) together with the measured amplitude frequency response of the 8GHz band-pass, 2GHz bandwidth, IF filter shown in figure 1. Figure 10b shows the original pulse in blue along with a theoretical output pulse after the IF filter in red. The latter was obtained by multiplying in the frequency domain the complex value of the filter response (amplitude and phase from VNA measurements) with the Fourier transform of a 650ps FWHM Gaussian pulse. The product is then inverse Fourier transformed to recover the resulting pulse in the time domain. Figure 10b shows the results of this calculation with the output pulse scaled and time-shifted to have the maxima of both pulses coincide in amplitude and time.

Although only a small portion of the pulse power lies outside the IF filter shape, this mismatch leads to two important consequences. First, figure 10b shows that the output pulse rise-time follows a Gaussian functional form, but it is wider by 100ps than the original. Second, figure 10b shows the right-hand side of the resulting pulse decays rapidly and features the ringing pulses. The fall-time of the pulse is faster than the original and not necessarily Gaussian. The main pulse is immediately followed by smaller pulses of amplitude up to $\sim 17\%$ that of the first pulse. This calculation has been repeated for a 250ps FWHM pulse leading to increased rise-time by $\sim$300ps and ringing pulses with amplitudes of $\sim$40%. In the case of a 2.5ns FWHM pulse, no ringing nor pulse-shape distortion was observed. The amount of rise-time increase and ringing strength are thus directly connected with the amout of pulse power lying outside the filter pass-band.

Fortunately, the rise-time increase does not affect group-delay measurements through either analog nor direct-sampling timing techniques since the Gaussian functional form is maintained. Any systematic errors caused by this increased pulse width are taken into account during HE-11 mirror calibrations performed before density profile measurements (see section IV D). Furthermore, by virtue of the constant IF frequency, all frequencies are affected equally by the IF filter shape. Unfortunately, because the increase in rise-time is dependant on the amount of shape mismatch, the experimental results of section **??** can only be considered preliminary and at best only indicative of true plasma-induced pulse width changes. Future analysis can include ringing pulse amplitudes to infer pulse widths based on this modeling results.

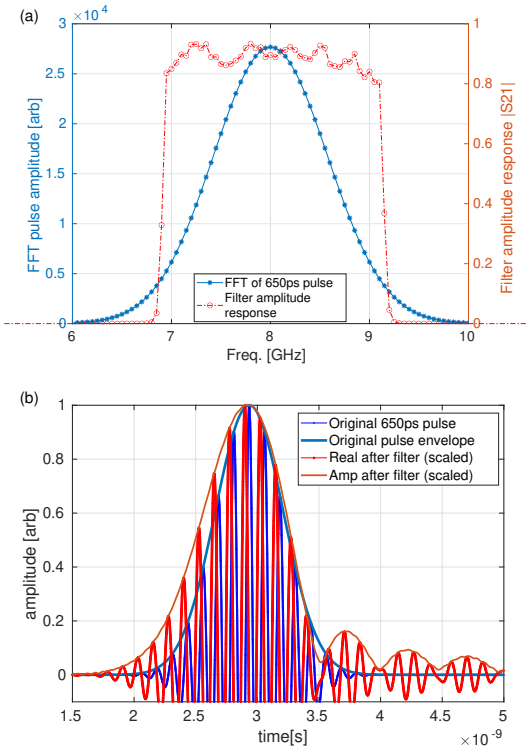

FIG. 10: Effects of pulse and IF filter shape mismatch. (a) 650ps FWHM pulse spectrum and 8GHz-2GHz bandwidth IF filter measured amplitude response. (b) Reconstructed pulse shape after propagation through the IF filter.

Lastly, figure 10 can be directly compared with figure 4. It is believed that the combined bandwidth of the elements between the filter and the timing circuit, namely: Schottky diode, pulse amplifier, and low-pass filter prevent the recorded pulse in figure 4 to feature the amplitude dip before the ringing pulse as seen in figure 10. These elements cause a smoother decay observed in figure 4. The ringing pulse is clearly observed in magenta. However, the ringing pulse amplitude is about 28% of the main pulse amplitude, larger than the model 17% in figure 10. This provides evidence for possible pulse compression in the receiver mixer: a 500ps FHWM input pulse would lead to a 780ps output pulse with ringing pulse amplitudes of 26%. These results encourage vividly a change in functional form and/or bandwidth in the IF filter for future diagnostic improvements.

[1]F. Clairet, C. Bottereau, A. Medvedeva, D. Molina, G. D. Conway, A. Silva, and U. Stroth. 1 micro second Broadband Frequency Sweeping Reflectometry for Plasma Density and Fluctuation Profile Measurements. *Review of Scientific Instruments*, 88(11), 2017.

[2]V F Shevchenko, A. A. Petrov, and V G Petrov. Pulse radar reflectometry for fusion plasma diagnostics. *International Journal of Infrared and Millimeter Waves*, 14(9):1755–1768, 1993.

[3]S. H. Heijnen. *Pulsed Radar Reflectometry - A new approach to measure electron densities in thermonuclear plasmas*. PhD thesis, Utrecht University, 1995.

[4]T. Tokuzawa, K. Kawahata, K. Tanaka, Y. Nagayama, LHD Experimental Group, T. Kaneba, and a. Ejiri. X-mode pulsed radar reflectometer for density fluctuation measurements on LHD. *Review of Scientific Instruments*, 74(3):1506, 2003.

[5]EJ Doyle, KW Kim, and JH Lee. Reflectometry applications to ITER. *Diagnostics for Experimental Thermonuclear Fusion Reactors*, pages 117–132, 1996.

[6]AJH Donné, SH Heijnen, and CAJ Hugenholtz. Pulsed radar reflectometry and prospects for fluctuation measurements. *Fusion engineering and design*, 35:73–80, 1997.

[7]S. Hacquin, S. Heuraux, M. Colin, and G. Leclert. Use of dispersive effects for density profile reconstruction from pulse radar reflectometry measurements alone. *Plasma Physics and Controlled Fusion*, 42(3):347–358, 2000.

[8]B. I. Cohen, T. B. Kaiser, and J. C. Garrison. One- and two-dimensional simulations of ultra-short-pulse reflectometry. *Review of Scientific Instruments*, 68(2):1238–1243, 1997.

[9]S. Hacquin, S. Heuraux, M. Colin, and G. Leclert. Fast computations of wave propagation in an inhomogeneous plasma by a pulse compression method. *Journal of Computational Physics*, 174(1):1–11, 2001.

[10]V. F. Shevchenko. Effect of Density Fluctuations on the Pulse Reflectometry of a Tokamak Plasma. *Plasma Physics Reports*, 23(2):151–157, 1996.

[11]D.R. Bolton, Cruisckshank P.A.S., D.A. Robertson, and G.M. Smith. Sub-nanosecond coherent pulse generation at millimetre-wave frequencies. *Electronic Letters*, 43(6), 2007.

[12]P. Molina Cabrera, S. Coda, L. Porte, N. Offeddu, P. Lavanchy, M. Silva, and M. Toussaint. V-band Doppler backscattering diagnostic in the TCV tokamak. *Review of Scientific Instruments*, 89(8):083503, 2018.

[13]Wolfgang Becker. The bh TCSPC Handbook. Technical Report 7th edition, Becker and Hickl GmbH., Berlin, 2017.

[14]Caen. Time Measurements with CAEN Waveform Digitizers. Technical report, CAEN, Viareggio, 2015.

[15]G. D. Conway. Scattering of reflectometer signals from rippled surfaces. *Review of Scientific Instruments*, 64(10):2782–2788, 1993.

[16]C Fanack, I Boucher, F Clairet, S Heuraux, G Leclert, and X L Zou. Ordinary-mode reflectometry: modification of the scattering and cut-off responses due to the shape of localized density fluctuations. *Plasma Physics and Controlled Fusion*, 38(11):1915–1930, 1999.

[17]Vladimir F. Shevchenko. Status and Prospects of Pulse Radar Reflectometry on the START tokamak. *Diagnostics for Experimental Thermonuclear Fusion Reactors*, 2, 1998.

[18]ME Manso, P Varela, and I Nunes. Reflectometry in conventional and advanced plasma scenarios on ASDEX Upgrade and perspectives for ITER. *Plasma physics and . . .*, 73, 2001.

[19]J.-M. Moret, F. Buhlmann, and G. Tonetti. Fast single loop diamagnetic measurements on the TCV tokamak. *Review of Scientific Instruments*, 74(11):4634–4643, 2003.

[20]A. Klein, H. Carfantan, D. Testa, A. Fasoli, and J. Snipes. A sparsity-based method for the analysis of magnetic fluctuations in unevenly-spaced Mirnov coils. *Plasma Physics and Controlled Fusion*, 50(12):1–17, 2008.

[21]D. Testa, A. Corne, G. Farine, C. Jacq, T. Maeder, and Matthieu Toussaint. 3D, LTCC-type, high-frequency magnetic sensors for the TCV Tokamak. *Fusion Engineering and Design*, 96-97(2):989–992, 2015.

[22]I.H. Hutchinson. *Principles of Plasma Diagnostics*. Cambridge University Press, New York, 2nd edition, 2002.

[23]P. Varela, M. E. Manso, A. Silva, J. Fernandes, and F. Silva. Initialization of plasma density profiles from reflectometry. *Review of Scientific Instruments*, 66(10):4937–4942, 1995.

[24]N. Vianello, C. Tsui, C. Theiler, S. Allan, J. Boedo, B. Labit, H. Reimerdes, K. Verhaegh, W. A.J. Vijvers, N. Walkden, S. Costea, J. Kovacic, C. Ionita, V. Naulin, A. H. Nielsen, J. Juul Rasmussen, B. Schneider, R. Schrittwieser, M. Spolaore, D. Carralero, J. Madsen, B. Lipschultz, and F. Militello. Modification

of SOL profiles and fluctuations with line-average density and divertor flux expansion in TCV. *Nuclear Fusion*, 57(11), 2017.

[25] O. E. Garcia, J. Horacek, R. A. Pitts, A. H. Nielsen, W. Fundamenski, V. Naulin, and J. Juul Rasmussen. Fluctuations and transport in the TCV scrape-off layer. *Nuclear Fusion*, 47(7):667–676, 2007.

[26] H J Hartfuss and Thomas Geist. *Fusion Plasma Diagnostics with mm-Waves - An Introduction*. Wiley-VCH - Physics Textbooks, 2013.

[27] Giorgia Dellaferrera. Covariance analysis and error measurement characterization of Tokamak equilibrium reconstruction. Technical report, Swiss Plasma Centre. Ecole Polytechnique Federale de Lausanne, Lausanne, Switzerland, 2018.

[28] H. Bottollier-Curtet and G. Ichtchenko. Microwave reflectometry with the extraordinary mode on tokamaks: Determination of the electron density profile of Petula-B. *Review of Scientific Instruments*, 58(4):539–546, 1987.

[29] R. B. Morales, S. Hacquin, S. Heuraux, and R. Sabot. New density profile reconstruction methods in X-mode reflectometry. *Review of Scientific Instruments*, 88(4), 2017.

[30] D. A. Shelukhin, V. A. Vershkov, G. F. Subbotin, D. V. Sarychev, A. A. Petrov, V. G. Petrov, M. M. Sokolov, and G. B. Igonkina. Measurements of electron density profile by frequency modulated continuous wave reflectometer in the T-10 tokamak using high magnetic field side probing and extraordinary mode lower cutoff. *Review of Scientific Instruments*, 89(9), 2018.